Descriptive modelling of food powders reconstitution kinetics followed by laser granulometry

Tristan Fournaise, Claire Gaiani, Jérémy Petit

Descriptive modelling of food powders reconstitution kinetics followed by laser granulometry

Tristan FOURNAISE[1], **Claire GAIANI**[1,2], **Jérémy PETIT**[1*]

[1]Université de Lorraine, LIBio, F-54000 Nancy, France.

[2]Institut Universitaire de France (IUF), France.

*corresponding author: jeremy.petit@univ-lorraine.fr

Abstract

Reconstitution kinetics of various food powders in fixed mixing conditions were followed by laser granulometry. Obtained reconstitution profiles were fitted using a sum of first-order indicial responses. This descriptive modelling approach allowed linking each of the main reconstitution steps (swelling, dispersion, and solubilization) to a single first-order indicial response and characterizing their kinetics. Initial, maximal, and final median particle sizes; swelling, dispersion, and solubilization durations and rates; as well as an overall reconstitution time, were calculated from model parameters. This descriptive modelling approach was not successful for instant powders or powders composed of several major components having well different kinetics for the same reconstitution steps. The durations and rates of reconstitution steps were correlated with physicochemical properties of investigated powders in order to evidence the most influencing properties on food powders reconstitution: contents in lipids, sugars, fibers, and water, surface hydrophobicity, and mostly median particle size at dry state.

Keywords

Reconstitution; kinetics; food powders; granulometry; descriptive modelling; physicochemistry

1. Introduction

Powder reconstitutability is one of the most important functional properties, as industrials need to manage reconstitution of powdered ingredients in their manufacturing processes. Besides, instantaneity of powdered food products is a crucial end-use functionality, as the time needed for the preparation of a food product is often one of the main choice criteria for consumers and industrials (Forny et al., 2011). A multitude of studies has been carried out to better understand the mechanisms involved in powder reconstitution, leading to a consensus on four kinetically-driven steps called wetting, swelling/sinking, dispersion, and solubilization steps (Forny et al., 2011; Fournaise et al., 2021; Mitchell et al., 2015; Schuck et al., 2012).

First, powder wetting occurs when particles come in contact with a liquid (aqueous solution in the case of food powders). Wettability is defined as the time needed to replace the air/solid interface by the liquid/solid interface (Forny et al., 2011; IDF, 1987).

Then, the swelling/sinking step takes place after the wetting step: the penetration of the liquid into individual particles or particle agglomerates increases their weight, leading to their immersion when the stress exerted on the liquid surface by the wet particle weight exceeds surface tension. Also, particle swelling may occur depending on the chemical composition of particles and this phenomenon can result in the formation of lumps in the case of cohesive powders (Forny et al., 2011; Jiang et al., 2013). Indeed, upon interaction with water, polymers of macromolecules (for food powders: mainly, proteins, starch, and fibers) swell, resulting in a softening of the particle outer layers and an increase in their size, leading to particle size increase (Bonacucina et al., 2009; Conti et al., 2006; Cuq et al., 2011; Forny et al., 2011). Fibers and starches are known to swell quickly due to their hydrophilic behavior, contrarily to proteins

which are more hydrophobic and thus have a low swelling rate (Eastman and Moore, 1984; Gaiani et al., 2007; Kravtchenko et al., 1999; Lamberti et al., 2004; Parker et al., 2000).

After particle wetting/swelling/sinking, powder dispersion occurs according to two main phenomena: deagglomeration which designates the disintegration of lumps and agglomerates into individual particles, and attrition which corresponds to the release of particle fragments by water-induced breaking (Fang et al., 2011; Forny et al., 2011; Mimouni et al., 2010). Particle attrition occurs when the cohesion between particle components (mainly by Van der Walls interactions and hydrogen bonds) is overwhelmed by shear stresses exerted by the liquid. Powders rich in proteins and/or lipids are known to be cohesive due to the hydrophobicity of these compounds (Cuq et al., 2011; Freudig et al., 1999; O'Mahony and McSweeney, 2016; Schuck et al., 2012).

Last, the solubilization step encompasses the dissolution of soluble components and the homogenization of insoluble components in the liquid. This leads to the complete loss of particle structure and the final reconstituted product consists in a suspension of insoluble components (Gaiani et al., 2007; Marabi et al., 2008; O'Mahony and McSweeney, 2016). The presence of proteins is known to decrease the solubilization rate, as interactions between them should be broken before proteins may be solubilized. Besides, fibers and starches generally contribute to increase the solubilization rate, as soluble fibers and starches are extremely hydrophilic and thus prone to solubilize, whereas insoluble fibers and starches are not susceptible to solubilize, which shortens the whole solubilization time (Gaiani et al., 2007; Kravtchenko et al., 1999; Yousefi et al., 2011). Based on diffusive models, it can be stated that small particles may solubilize faster, owing to their higher specific surface area (Dokoumetzidis and Macheras, 2006; Nernst, 1904).

Despite the consensus on the identification of the reconstitution steps, the characterization of their kinetics still remains a real challenge. Indeed, for some powders, wetting and dispersion

steps may be almost instantaneous, precluding the possibility to determine their kinetics owing to limitations in acquisition frequency of analytical equipments. Also, for many powders, some of the reconstitution steps may overlap (for instance, when the particle outer layer begins to solubilize before that dispersion or even swelling steps may have been finished), making it difficult to deconvolute the respective influences of each step (Forny et al., 2011).

Countless methods have been used to identify and characterize powder reconstitution steps: direct methods in which particle size estimators are followed, like focused beam reflectance measurement, image analysis, and laser diffraction; and indirect methods such as turbidimetry, acoustic spectroscopy, or conductimetry (Bonacucina et al., 2009; Fournaise et al., 2021; Galet et al., 2004, 2004; Goalard et al., 2006; Li et al., 2013; Marabi et al., 2008). In a previous work, powder reconstitution kinetics followed by conductimetry have been described by a sigmoidal-shaped Hill function that allowed an accurate determination of the reconstitution time (Fournaise et al., 2021). However, this method did not provide information about kinetics of each reconstitution step. In the literature, several methods have been developed to focus on reconstitution steps by a single particle approach: for instance, swelling of a single particle of superabsorbent polymers has successfully been characterized (Sweijen et al., 2017). Moreover, the dispersion and solubilization steps were described by first-order models such as the Noyes-Whitney equation, the Hopfenberg model, or the Higuchi model (Dokoumetzidis and Macheras, 2006; Higuchi, 1961; Hopfenberg, 1976; Noyes and Whitney, 1897; Richard, 2012).

The aim of the present study was to develop a general model able to describe in a single equation the evolution of median particle size when reconstituting food powders, which can be used to identify the reconstitution times of various food powders with a good accuracy by calculations based on the reconstitution curve. The developed descriptive model was designed to obtain information about the different reconstitution steps by choosing an appropriate mathematical form (first-order indicial responses). This permitted to determine the switching points from one

predominant step to another, as well as an average evolution rate of median particle size during each step. Last, characteristic parameters of reconstitution steps issued from the descriptive model were interpreted to identify the most influent powder physicochemical properties on each reconstitution step.

2. Material and methods

2.1. Food powders

Industrial food powders varying in median particle size, particle structure, chemical composition, surface hydrophobicity, etc. (Table 1) were employed for reconstitution assays. Powder physicochemical properties of instant mash, casein, polenta 1.0 mm, small couscous, T55 and T45 flours, cocoa fat- alka-, cocoa fat+ alka+, MPI, and instant coffee were obtained from a previous study (Fournaise et al., 2021).

Table 1: Physicochemical characteristics of investigated powders (adapted from Fournaise et al., 2021).

Sample name	Commercial name	Supplier (country)	Protein content (g/100 g*)	Lipid content (g/100 g*)	Content in carbohydrates, sugars and fibers excluded (g/100 g*)	Sugar content (g/100 g*)	Fiber content (g/100 g*)	Mineral content (g/100 g*)	Water content (g/100 g*)	Water activity (-)	C/O ratio (-)	C-C/other C bonds ratio (-)	Dry median particle size (µm)
Instant mash	Instant mashed potatoes	Pom'Lisse (France)	8.1	0.6	80.1	0.7	8.4	0.08	2.1	0.37	3.44	1.11	482
Casein	Micellar casein powder	Ingredia (France)	86	1.6	0.0	2.1	0.0	8.8	1.6	0.25	3.90	1.41	53.8
Polenta 1.0 mm	Polenta	Leclerc (France)	7.7	2.0	83.7	0.8	2.8	0.01	3.0	0.55	3.97	1.29	392
Small couscous	Fine couscous powder	Comptoir du Grain (France)	13.2	2.0	76.9	2.7	2.6	0.04	2.6	0.52	4.97	1.25	975
T55 flour	T55 flour	Tablier Blanc (France)	13.1	1.3	75.8	0.6	6.0	0.03	3.1	0.54	4.19	1.54	87.9
T45 flour	T45 flour	Leclerc (France)	13.1	1.3	75.6	0.6	6.0	0.03	3.4	0.55	4.17	1.47	87.7
Cocoa fat- alka-	12 % fat not alkalized cocoa	Bensdorp (U.S.A.)	25.4	12.2	20.5	0.6	38.2	2.1	0.9	0.27	4.29	2.12	12.7
Cocoa fat+ alka+	23 % fat lightly alkalized cocoa	Bensdorp (U.S.A.)	21.5	25.3	17.6	0.4	32.9	1.5	0.8	0.18	5.09	2.80	29.4
MPI	Milk protein isolate	Ingredia (France)	89.1	1.6	1.0	1.0	0.0	6.7	1.5	0.25	4.06	1.08	54.2
Instant coffee	Instant coffee	Carte d'Or (France)	21.1	6.2	53.6	0.0	8.2	9.2	1.7	0.16	2.80	0.92	1 633

*on wet basis

2.2. Determination of median particle size at dry state by laser granulometry

Particle size distribution was determined in a previous study (Fournaise et al., 2021) with a Mastersizer 3000 laser granulometer (Malvern Instruments Ltd., Malvern, UK) supplied with a red light 4 mW He-Ne laser and a blue light 10 mW LED respectively operating at 632.8 and 470.0 nm wavelengths with a 300 RF lens. Dry dispersion (Aero S module, Malvern) conditions were used: 2 mm hopper length, 35 % feed rate, and 2 bar air pressure. The chosen particle size estimator was the diameter in volume of a sphere of equal projection area. The median particle size D50, a classical granulometric parameter which corresponds to the diameter for which 50 % of the particle population have smaller sizes, was used to characterize powder samples.

2.3. Monitoring of reconstitution kinetics by laser granulometry using wet dispersion

The monitoring of food powder reconstitution kinetics was carried out with the same Mastersizer 3000 laser diffraction granulometer using wet dispersion. Reconstitution conditions were similar for all powders: 0.1 g powder was quickly poured into 125 mL distilled water at 25 °C in the Hydro MV module (Malvern) stirred at 2 000 rpm. Powder reconstitution was followed until reaching D50 stability, i.e., for durations ranging from 15 min to 2 h depending on the investigated powder, by acquiring 1 s measurement on both lasers every 5 s. The curve displaying the temporal evolution of the median particle size D50, called reconstitution curve hereafter, was built by averaging results obtained for three replicates of reconstitution assays. Figures 1A displays the reconstitution curve obtained for instant mash as an example.

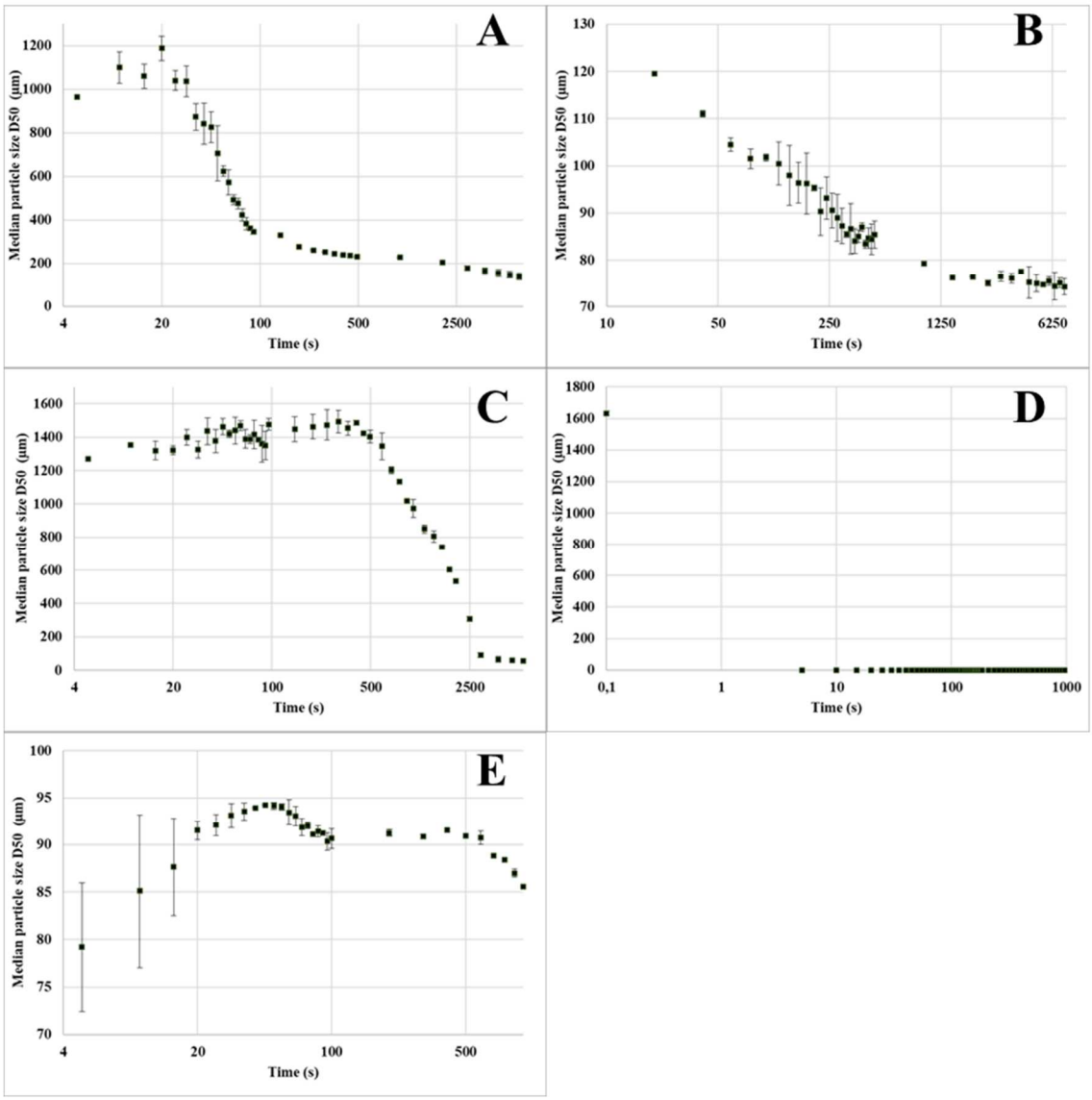

Fig. 1: Reconstitution curves obtained by monitoring or reconstitution assays with laser granulometry, with temporal axis in logarithmic scale. (A) instant mash (first reconstitution type); (B) T45 flour (second reconstitution type); (C), small couscous (third reconstitution type); (D) instant coffee (fourth reconstitution type); (E) MPI (fifth reconstitution type). Error bars indicate standard deviations obtained with three replicates of reconstitution assays; some, inferior to the marker size, are not visible.

2.4. Descriptive model of food powder reconstitution

2.4.1. Types of reconstitution curves

The median particle size is expected to increase during the wetting and sinking/swelling steps (abbreviated in swelling step hereafter), then to decrease in the dispersion and solubilization

steps at different kinetic rates, corresponding to a slope change in the reconstitution curve. For some investigated powders such as instant mash (Figure 1A), the observation of reconstitution curves (with temporal axis in logarithmic scale for a better identification of times at which slope changes occurred) allowed to identify the successive predominance of the three main reconstitution steps. This reconstitution behavior was called the first reconstitution type and could be described by the model developed in this study.

Some powders, for instance T45 flour (Figure 1B) exhibited no particle size increase at the beginning of the reconstitution assay, because no swelling occurred or it was too insignificant or too quick to be accurately monitored by laser granulometry. These powders were considered to belong to the group of second reconstitution type and their reconstitution could also be modelled using the approach of the present study.

For some powders like small couscous (Figure 1C), a swelling step was present in reconstitution curves but no slope change was detected. This may happen with powders for which:

- one of the dispersion or solubilization steps was too quick to be accurately monitored by laser granulometry,

- one of the dispersion and solubilization steps overwhelmed the impact of the other step,

- or powders for which dispersion and solubilization steps had similar kinetics.

This reconstitution behavior was named the third reconstitution type and the model developed in the present paper was also able to describe its kinetics.

For instant coffee (Figure 1D), reconstitution occurred too quickly to be accurately monitored by laser granulometry owing to acquisition frequency limitations. In this case, defined as the fourth reconstitution type, reconstitution steps could not be distinguished and the modelling approach developed in this study was not suitable to evaluate reconstitution kinetics.

The fifth reconstitution type was defined for powders leading to accurate reconstitution curves but too complex to be modelled by the descriptive modelling approach of the current study, which decouples the three main reconstitution steps but is not able to take into account multiple kinetics for a given step. Among investigated powders, this was the case for milk protein isolate (Figure 1E) for which the reconstitution curve exhibited a first increase, then a first decrease, followed by a second increase and a second decrease.

2.4.2. Descriptive modelling approach

The aim of the descriptive modelling approach developed in this study was to determine a single-equation model able to describe the temporal evolution of the median particle size D50 upon reconstitution. This model was intended to identify the kinetics of each of the three main reconstitution steps detected on reconstitution curves, namely swelling, dispersion, and solubilization steps. A sum of three first-order indicial responses (Eq. (1)) was employed with the objective to link each first-order indicial response to a single reconstitution step.

$$\mathrm{D50}(t) = \mathrm{D50}_0 + \mathrm{A}_0\left(1 - \mathrm{e}^{\frac{-t}{\tau_0}}\right) - \mathrm{A}_1\left(1 - \mathrm{e}^{\frac{-t}{\tau_1}}\right) - \mathrm{A}_2\left(1 - \mathrm{e}^{\frac{-t}{\tau_2}}\right) \quad (1)$$

Where:

- $\mathrm{D50}_0$ (µm): modelled initial median particle size at wet state;
- A_0 (µm): amplitude of the increasing first-order indicial response (swelling step);
- τ_0 (s): time-constant of the increasing first-order indicial response (swelling step);
- A_1 (µm): amplitude of the first decreasing first-order indicial response (dispersion step);
- τ_1 (s): time-constant of the first decreasing first-order indicial response (dispersion step);
- A_2 (µm): amplitude of the second decreasing first-order indicial response (solubilization step);

- τ_2 (s): time-constant of the second decreasing first-order indicial response (solubilization step).

For powders of the first reconstitution type, model parameters were expected to be all different from zero, whereas A_0 was fixed at 0 µm for powders of the second reconstitution type (leading to a sum of two decreasing first-order indicial responses), and A_2 was fixed at 0 µm for powders of the third reconstitution type (leading to a sum of two first-order indicial responses, the first one increasing and the other one decreasing).

The reconstitution curves of powders of first, second, and third reconstitution types were fitted with the Excel solver (Microsoft 365) using the least squares method solved by the generalized reduced gradient algorithm. Direct fitting of the whole reconstitution curve with Eq. (1) was judged unsatisfactory (data not shown) for many reasons:

- sometimes the fitting method did not converge,

- when fitting was achieved, modelled initial median particle size at wet state $D50_0$ was often inferior to the median particle size at dry state, which was not physically sound,

- and/or calculated durations of each reconstitution step seemed to be unrelated to what could be deduced from the observation of reconstitution curves.

Thus, a descriptive modelling approach that was successful for all powders of first, second, and third reconstitution types and led to physically-sound and consistent estimations of initial median particle size at wet state and durations of each reconstitution step was developed. First, the increasing and decreasing parts of the reconstitution curves were separately fitted; then, the complete model was fitted by using the first estimation of model coefficients deduced by separate fittings for the initialization of model parameters.

214 2.4.2.1. Separate fitting of the increasing and decreasing parts of the reconstitution
215 curve

216 For first and third reconstitution type powders, the increasing part of the temporal evolution of
217 the median particle size from its initial value to its maximal value, corresponding to the
218 predominance of the swelling step, was fitted with an increasing first-order indicial response
219 (Eq. (2)) by specifying the constraint that the modelled initial median particle size $D50_0^*$ should
220 be superior or equal to the median particle size at dry state. Indeed, at the beginning of
221 reconstitution, it was considered that particles could have swelled or agglomerated (upon
222 wetting and immersion) but their size could not be smaller to the dry median particle size, as
223 no significant erosion or solubilization was expected in such a short water-contact time (few
224 seconds). The fitting procedure performed with the Excel solver was initialized with the median
225 particle size at dry state for $D50_0^*$, and rough graphical estimations of the extent of median
226 particle size evolution and the time needed for this evolution for A_0 and τ_0, respectively.

227 $$D50(t) = D50_0^* + A_0\left(1 - e^{\frac{-t}{\tau_0}}\right) \quad (2)$$

228 Where $D50_0^*$ (µm) stands for the modelled initial median particle size D50 using Eq. (2) only.

229 For powders of the second reconstitution type, for which no swelling was observed, this part
230 of the modelling approach was obviously not performed.

231 The decreasing part of the temporal evolution of the median particle size, from its maximal
232 value to its final value, corresponding to the dispersion and solubilization steps, was modelled
233 by the sum of two decreasing first-order indicial responses (Eq. (3)) for powders of the first and
234 second reconstitution types (for which a slope change was observed in the decreasing part of
235 the reconstitution curve). The fitting procedure performed with the Excel solver was initialized
236 with the experimental maximal median particle size for $D50_1$, and rough graphical estimations

of the extents of median particle size evolution and the times needed for these evolutions during dispersion and solubilization steps for A_1, τ_1, A_2, and τ_2, respectively.

$$D50(t) = D50_1 - A_1\left(1 - e^{\frac{-t}{\tau_1}}\right) - A_2\left(1 - e^{\frac{-t}{\tau_2}}\right) \quad (3)$$

Where $D50_1$ (µm) designates the modelled initial median particle size D50 using Eq. (3) only.

The same equation was employed with A_2 fixed at 0 µm for third reconstitution type powders (for which no distinction could be made between dispersion and solubilization steps), leading to a single decreasing first-order indicial response.

2.4.2.2. Fitting of the complete model from the whole reconstitution curve

Then, the whole reconstitution curve was fitted with Eq. (1) by using the model parameters obtained by separate fitting with Eq. (2) and (3) ($D50_0^*$, A_0, τ_0, A_1, τ_1, A_2, and τ_2) to initiate the fitting procedure performed with the Excel solver.

As previously indicated, A_0 was fixed at 0 µm for powders of the second reconstitution type and A_2 was fixed at 0 µm for powders of the third reconstitution type.

Obtained model parameters ($D50_0$, A_0, τ_0, A_1, τ_1, A_2, and τ_2) were then used to calculate characteristic swelling, dispersion, and reconstitution times, as well as swelling, dispersion, and solubilization rates.

2.4.3. Estimation of the duration and the particle size evolution rate of each reconstitution step from the descriptive reconstitution model

The swelling time $t_{swelling}$ was defined as the time for which the predominance of the swelling mechanism ends. When applicable, it was calculated as the time at which modelled median

particle size reached its maximal value $D50_{max}$. This was determined with the Excel solver as the lowest time value for which the first derivative of D50(t) (Eq. (4)) was equal to zero.

$$\frac{dD50(t)}{dt} = -\frac{A_0}{\tau_0} e^{\frac{-t}{\tau_0}} + \frac{A_1}{\tau_1} e^{\frac{-t}{\tau_1}} + \frac{A_2}{\tau_2} e^{\frac{-t}{\tau_2}} \quad (4)$$

Thus, the maximal median particle size $D50_{max}$ was equal to $D50(t_{swelling})$ and the duration of the swelling-dominated reconstitution phase $\Delta t_{swelling}$ was equal to $t_{swelling}$.

The dispersion time $t_{dispersion}$, when applicable, was calculated as the time for which the absolute difference between experimental values and the reconstitution model considering that the swelling step was completely ended (i.e., it has induced an increase in the median particle size up to $D50_0 + A_0$) and taking into account the influence of the dispersion step only $D50_0 + A_0 - A_1\left(1 - e^{\frac{-t}{\tau_1}}\right)$ became superior to the absolute difference between experimental values and the reconstitution model considering that the swelling and dispersion steps were completely ended (i.e., they have induced an evolution of the median particle size up to $D50_0 + A_0 - A_1$) and taking into account the influence of the solubilization step only $D50_0 + A_0 - A_1 - A_2\left(1 - e^{\frac{-t}{\tau_2}}\right)$. Thus, the duration of the dispersion-dominated reconstitution phase $\Delta t_{dispersion}$ was equal to the difference between the dispersion and swelling times ($t_{dispersion} - t_{swelling}$).

The final median particle size $D50_\infty$ was equal to the limit of D50(t) when the time tends to the infinity, i.e., $D50_0 + A_0 - A_1 - A_2$. It was chosen to define the reconstitution time as the time needed to reach 95 % of the median particle size decrease in the dispersion and solubilization steps (Eq. (5)).

$$D50(t_{reconstitution}) = 95\ \% \times D50_\infty + 5\ \% \times D50_{max} \quad (5)$$

Hence, the duration of the solubilization-dominated reconstitution phase $\Delta t_{solubilization}$ was equal to the difference between the dispersion and swelling times ($t_{solubilization} - t_{dispersion}$).

Characteristic particle size evolution rates during swelling, dispersion, and solubilization steps were calculated as slopes at half height of the considered reconstitution step using the first derivative of D50(t) (Eq. (4)) and the Excel solver for the determination of half-height times of each reconstitution step:

- the swelling rate (positive value) was defined as the value taken by first derivative of D50(t) at the time (inferior to $t_{swelling}$) when modelled D50 reached $\frac{D50_0+D50_{max}}{2}$,

- the dispersion rate (negative value) was calculated as the value taken by first derivative of D50(t) at the time (comprised between $t_{swelling}$ and $t_{dispersion}$) when modelled D50 reached $\frac{D50_{max}+D50(t_{dispersion})}{2}$,

- and the solubilization rate (negative value) was the value taken by first derivative of D50(t) at the time (superior to $t_{dispersion}$) when modelled D50 reached $\frac{D50(t_{dispersion})+D50_{\infty}}{2}$.

2.5. Statistical analysis

Reconstitution assays were triplicated to ensure good analytical repeatability and obtain good accuracy of descriptive reconstitution models. The duration and the median particle size evolution rate of each reconstitution step were correlated with powder physicochemical properties by calculating Pearson's correlation coefficients with Microsoft 365 Excel ($p < 0.05$).

3. Results

3.1. Application of the two-step fitting approach of the descriptive reconstitution model: example of instant mash

302 Reconstitution curve of instant mash (Fig. 1A) was of first type (distinguishable swelling,
303 dispersion, and solubilization steps). The experimental median particle size first increased from
304 481 µm to 1 188 µm between time zero and about 20 s, corresponding to the swelling step.
305 Then, it decreased from 1 188 µm to 109 µm from about 20 s to the end of the reconstitution
306 assay, which was associated with the dispersion and solubilization steps. The slope change in
307 the decreasing part of the reconstitution curve indicated that dispersion took place between 20
308 and 100 s approximately, and solubilization was the dominant reconstitution mechanism above
309 circa 100 s.

310 Thus, the separate fitting of increasing and decreasing parts of the reconstitution curve was
311 carried out following the procedure described in subsection 2.4.2.1. The swelling-dominated
312 reconstitution phase only (increasing part) was modelled with Eq. (2) with $D50_0^* = 482$ µm,
313 $A_0 = 623$ µm, $\tau_0 = 3.2$ s, and $R^2 = 95.8$ % (Fig. (2)).

314

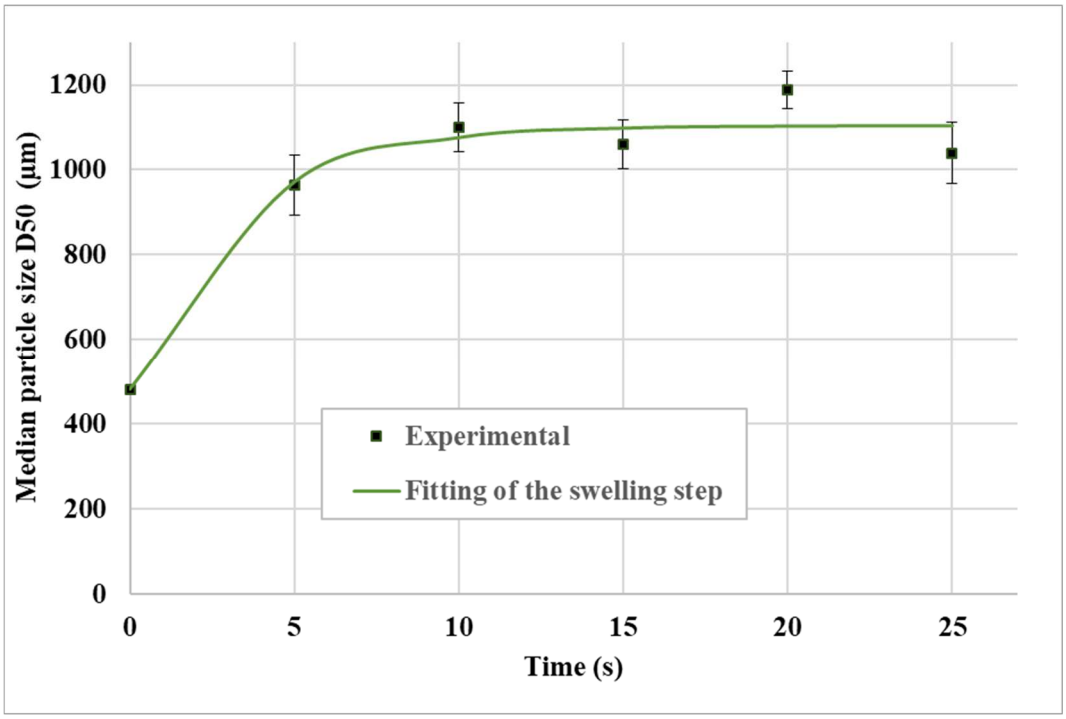

315

316 Fig. 2: Separate fitting of the swelling step of the (first type) reconstitution profile of instant mash using Eq. (2).
317 Error bars indicate standard deviations obtained with three replicates of reconstitution assays; some, inferior to the
318 marker size, are not visible.

319

320 The dispersion- and solubilization-dominated reconstitution phases only (decreasing part) were
321 modelled with Eq. (3) with $D50_1$ = 1 939 µm, A_1 = 1 687 µm, τ_1 = 35.9 s, A_2 = 153 µm,
322 τ_2 = 4 990 s, and R^2 = 98.9 % (Figure 3).

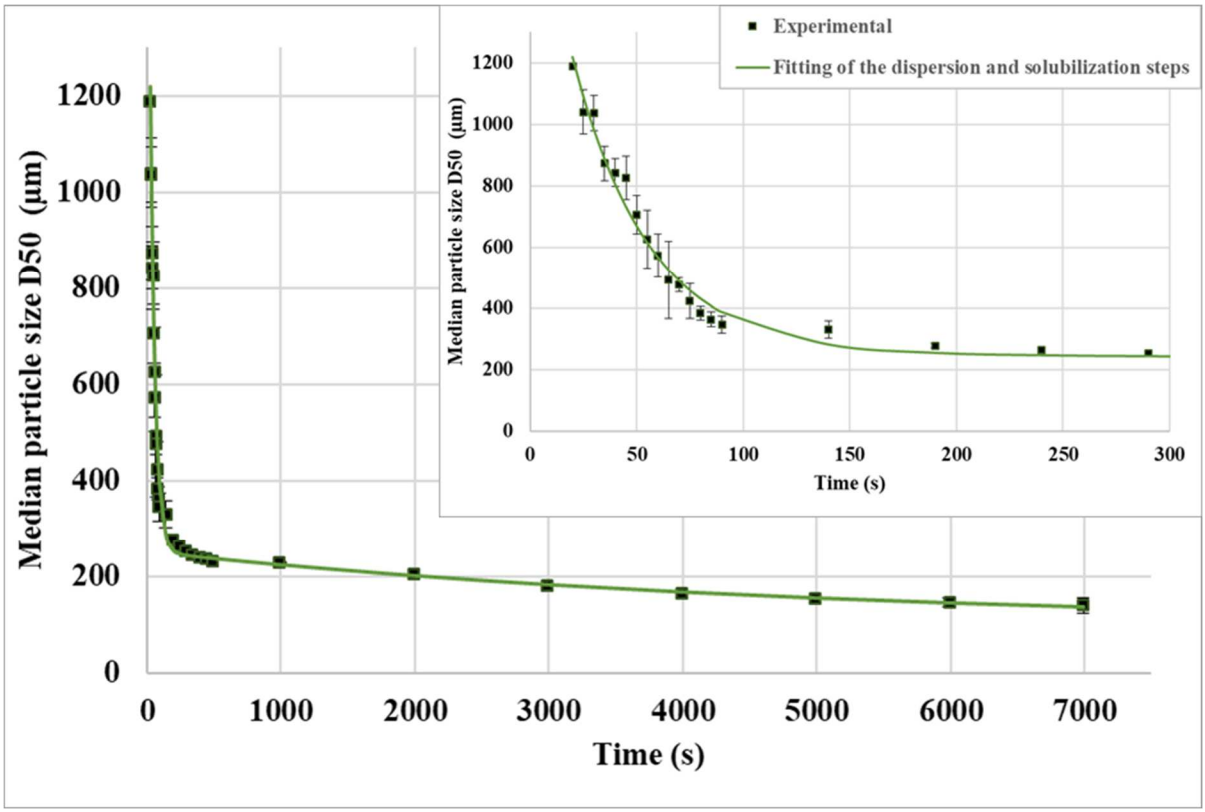

Fig. 3: Separate fitting of the dispersion and solubilization steps of the (first type) reconstitution profile of instant mash using Eq. (3). Error bars indicate standard deviations obtained with three replicates of reconstitution assays; some, inferior to the marker size, are not visible.

The last step of the fitting approach consisted in modelling the whole reconstitution curve using Equation (1) following the procedure described in subsection 2.4.2.2, resulting in $D50_0 = 653$ µm, $A_0 = 4\ 297$ µm, $\tau_0 = 16.0$ s, $A_1 = 4\ 695$ µm, $\tau_1 = 24.8$ s, $A_2 = 153$ µm, $\tau_2 = 4\ 990$ µm, and $R^2 = 99.3$ %. The obtained descriptive model was in great accordance with the reconstitution curve (Fig. 4), as denoted by the elevated coefficient of determination R^2.

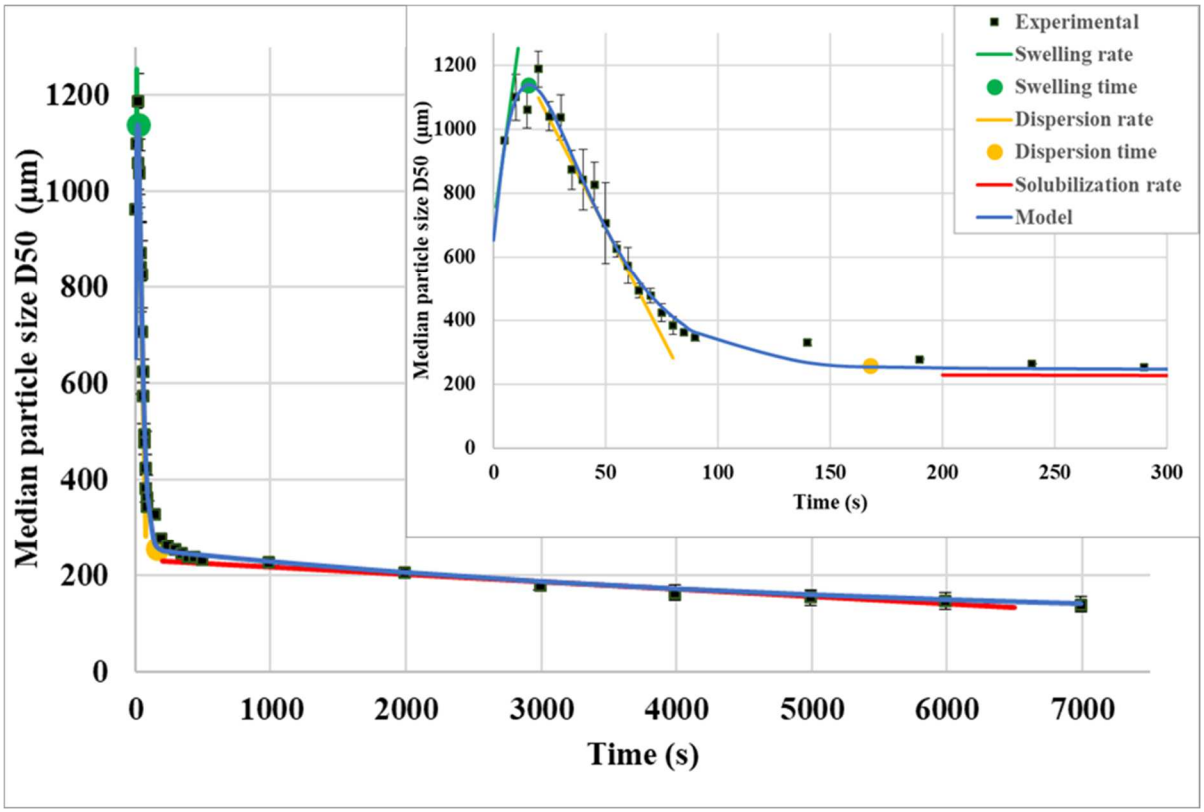

Fig. 4: Descriptive reconstitution model for instant mash obtained by fitting with Eq. (1); swelling and dispersion times; swelling, dispersion, and solubilization rates. Error bars indicate standard deviations obtained with three replicates of reconstitution assays; some, inferior to the marker size, are not visible.

Following the procedure described in subsection 2.4.3., the complete reconstitution model was used to calculate modelled initial, maximal, and final median particle sizes; swelling, dispersion, and solubilization durations and rates; as well as reconstitution time: $D50_0$ = 653 µm, $D50_{max}$ = 1 139 µm, $D50_\infty$ = 103 µm, $\Delta t_{swelling}$ = 15.7 s, $\Delta t_{dispersion}$ = 152 s, $\Delta t_{solubilization}$ = 5 222 s, $t_{reconstitution}$ = 5 390 s, +49.6 µm.s^{-1} swelling rate, -13.6 µm.s^{-1} dispersion rate, and -0.015 µm.s^{-1} solubilization rate.

3.2. Influence of physicochemical properties on powder reconstitution steps

The modelling approach following the procedure described in section 2.4 permitted to obtain the descriptive reconstitution models displayed in Figures S1, S2 and S3 (cf. supplementary material) when applied to the first, second, and third types of reconstitution curves of investigated powders. Model parameters; initial, maximal, and final median particle sizes; swelling, dispersion, and solubilization durations and rates; as well as reconstitution time are listed in Table 2.

Table 2: Modelled initial, maximal, and final median particle sizes; model parameters and coefficient of determination; swelling, dispersion, and solubilization durations and rates; reconstitution time of investigated powders of the first (instant mash, casein, and polenta 1.0 mm), second (T55 flour, T45 flour, cocoa fat- alka-, and cocoa fat+ alka+), and third reconstitution types (small couscous).

Type of reconstitution curve (cf. subsection 2.4.1)		Sample	$D50_0$ (µm)	$D50_{max}$ (µm)	$D50_\infty$ (µm)	A_0 (µm)	τ_0 (s)	A_1 (µm)	τ_1 (s)	A_2 (µm)	τ_2 (s)	R^2 (%)	Swelling duration (s)	Dispersion duration (s)	Solubilization duration (s)	Reconstitution time (s)	Swelling rate (µm/s)	Dispersion rate (µm/s)	Solubilization rate (µm/s)
	First	Instant mash	653	1 139	103	4 297	16.0	4 695	24.8	153	4 990	99.3	15.7	152	5 222	5 390	+49.6	-13.6	-1.5×10^{-2}
		Casein	53.8	105	40.4	69.4	8.5	23.5	30.3	59.2	1 473	99.8	26.2	35.1	4 216	4 278	+4.0	-0.17	-2.0×10^{-2}
		Polenta 1.0 mm	392	515	262	153	15.6	113	274	170	1 752	99.0	48.6	304	4 204	4 556	+5.1	-0.30	-5.2×10^{-2}
	Second	T55 flour	110	110	67.8	/*	/*	21.9	80.9	20.7	903	97.7	/*	155	1 897	2 052	/*	-0.17	-1.1×10^{-2}
		T45 flour	130	130	75.6	/*	/*	20.9	30.6	33.5	320	98.6	/*	46,6	756	803	/*	-0.57	-5.4×10^{-2}
		Cocoa fat- alka-	24.7	24.7	13.8	/*	/*	7.0	17.2	3.9	412.6	99.8	/*	48.0	765	813	/*	-0.22	-4.7×10^{-3}
		Cocoa fat+ alka+	37.7	37.7	22.1	/*	/*	8.2	82.5	7.4	1 334	99.1	/*	179	2 824	3 004	/*	-5.8×10^{-2}	-2.7×10^{-3}
	Third	Small couscous	1 324	1 481	17.4	993	288	2 299	1 244	/*	/*	99.1	234	/*	4 054	4 288	+1.0	-0.57**	

*: not applicable.

**: dispersion/solubilization rate.

With the modelling approach developed in this study, the information about reconstitution kinetics of food powders was gathered in the characteristic parameters calculated from the descriptive reconstitution model (Table 2), each parameter being associated with one reconstitution step only. The obtained descriptive model was not built to predict the durations and rates of reconstitution steps from powder physicochemical properties (bulk and surface chemical compositions, granulometric characteristics) and reconstitution conditions (e.g., stirring speed, impeller type, volume and geometry of the reconstitution reactor, powder/water mass ratio, water temperature), but the characteristic parameters of each reconstitution step calculated from the descriptive model can still be used to establish correlations with powder physicochemistry and reconstitution conditions. However, in this study, the latter were fixed and their influence on reconstitution steps could therefore not be evaluated. Thus, powder physicochemical parameters that had the most influence on powder reconstitution kinetics were identified by calculating Pearson's correlation coefficients (Table 3).

Table 3: Pearson's correlation coefficients between powder physicochemical properties (bulk and surface chemical compositions, granulometric characteristics) and reconstitution characteristic parameters (swelling, dispersion, and solubilization durations and rates; reconstitution time issued from the descriptive modelling approach).

Pearson's correlation coefficients (R)	Protein content	Lipid content	Content in carbohydrates, sugars and fibers excluded	Sugar content	Fiber content	Mineral content	Water activity	Water content	C/O ratio	C-C/other C bonds ratio	Dry median particle size
Swelling rate (µm/s)	-0.35	-0.96	0.31	-0.64	0.92	-0.31	-0.16	-0.26	-0,70	-0.81	-0.04
Swelling duration (s)	-0.30	0.56	0.31	-0.74	-0.22	-0.36	0.55	0.38	0.96	-0.02	0.87
Dispersion rate (µm/s)	0.28	0.29	-0.38	0.10	0.16	0.25	0.02	0.01	0.64	0.45	-0.74
Dispersion duration (s)	-0.54	0.06	0.51	-0.35	-0.15	0.04	0.34	0.32	0.03	-0.08	0.61
Solubilization rate (µm/s)	0.20	0.55	-0.55	-0.07	0.61	0.22	-0.72	-0.74	0.30	0.52	-0.34
Solubilization duration (s)	0.19	-0.23	0.09	0.42	-0.45	0.23	-0.13	0.01	-0.51	-0.45	0.72
Reconstitution time (s)	0.11	-0.26	0.17	0.44	-0.49	0.13	-0.02	0.07	-0.27	-0.48	0.59

Green:highly significant correlations; orange: significant correlations; red: insignificant correlations.

As for powder swelling, both the dry median particle size and particle surface hydrophobicity (C/O ratio) were positively correlated with the swelling duration. This influence of median particle size on the time needed for powder swelling was expected as the prior mechanism of water uptake should be slower for large particles owing to their lower specific surface area. Besides, surface hydrophobicity may delay powder wetting and sinking, resulting in larger swelling duration (as wetting and sinking were considered as included in swelling step in the descriptive modelling approach developed in the present study). The swelling duration was also decreased at higher sugar content, which was logical as sugars quickly disperse and solubilize without observable swelling. Swelling was also significantly influenced by lipid and fiber contents along with particle surface hydrophobicity (C-C/other C bonds ratio): the presence of fibers increased the swelling rate owing to their hydrophilic nature (Bonacucina et al., 2009; Conti et al., 2006; Cuq et al., 2011; Kravtchenko et al., 1999). On the contrary, the presence of lipids and a higher surface hydrophobicity (denoted by a greater C-C/other C bonds ratio) tend to decrease the swelling rate due to limitation of surface wetting and water transfer into the particle (Fournaise et al., 2021, 2020; Gaiani et al., 2007; Kim et al., 2002; Murrieta-Pazos et al., 2012).

Then, a positive correlation was found between the dispersion rate and particle surface hydrophobicity evaluated by the C/O ratio, which means that an increase in surface hydrophobicity led to a slower dispersion (as dispersion rates are negative values). This can be explained by the low degree of interaction of water with hydrophobic particle surface that is detrimental to the breaking of intraparticular hydrogen bonds and van der Waals interactions involved in powder dispersion (Cuq et al., 2011; Fournaise et al., 2021; Freudig et al., 1999). On the opposite, a negative correlation was obtained between the dispersion rate and the median particle size, which means that a larger median particle size enhanced powder dispersion. This

may be due to the lower cohesion of large particles, facilitating their dispersion by water (Enferad et al., 2021; Gnagne et al., 2017; Salameh et al., 2016).

Solubilization was slowed by the presence of insoluble components such as fibers, as denoted by the positive correlation between the solubilization rate (negative values) and fiber content. Water retention by insoluble fibers may explain this slowing of solubilization in the presence of insoluble components. On the contrary, water content was negatively correlated with the solubilization rate (negative values), showing that a higher water content tended to enhance solubilization. The same observation was made for water activity. The improvement of solubilization for powders richer in water may be explained by their probable higher hydrophily. Also, it was noticed by calculation of Pearson's correlation coefficients between water content and lipid or fiber contents (respectively equal to -0.68 and -0.63) that powders richer in water contained less lipids and fibers. Thus, the enhancement of solubilization at higher water content may also be indirectly viewed as the consequence of the reduced presence of compounds deleterious for powder solubilization. Last, solubilization duration was increased for larger particles, which can be explained by the fact that their specific surface area than for smaller particles, the release of soluble compounds from larger particles takes longer (Dokoumetzidis and Macheras, 2006; Fournaise et al., 2021; Lamberti et al., 2004; Nernst, 1904).

In this study, the powder physicochemical property that exhibited the higher degree of correlation with reconstitution time was the dry median particle size ($R = 0.59$), showing that powder composed of larger particles may take more time to reach complete reconstitution. Indeed, an increase in particle size is known to favor powder wetting and dispersion, but large particles lead to longer swelling and solubilization steps (Dokoumetzidis and Macheras, 2006; Nernst, 1904).

4. Conclusion

This study presents a new descriptive modelling approach for food powder reconstitution. The proposed model permits to describe the temporal evolution of median particle size upon reconstitution and characterize the kinetics of the main substeps of powder reconstitution, namely swelling, dispersion, and solubilization. This approach made it possible to determine mean swelling, dispersion, and solubilization durations and rates, as well as reconstitution time. This descriptive modelling approach was not successful for instant powders (their reconstitution being too quick to be followed by laser granulometry) or powders composed of several major components having well different kinetics for the same reconstitution steps. The kinetic data obtained from this descriptive modelling approach were linked to powder physicochemistry (median particle size, span, bulk chemical composition, surface hydrophobicity) to identify the main physicochemical properties influencing each reconstitution step. Swelling lasted longer for powders composed of large particles and/or particles with a hydrophobic surface but it was shorter in the presence of sugars, whereas the swelling rate was enhanced in the presence of fibers and decreased in the presence of lipids. Dispersion was facilitated for large, whereas it was impaired by particle surface. Solubilization was slowed down in the presence fibers, and for large particles due to their lower specific surface area. Overall, these trends were consistent with literature knowledge, showing the relevancy of the developed descriptive modelling approach. Further works should apply the developed descriptive model to a greater number of investigated powders and focus on the influence of operating parameters of the reconstitution process (stirring speed, geometry, powder/water mass ratio, etc.). The identification of the most influent powder physicochemical properties and reconstitution conditions is a necessary step for the future development of empirical models able to predict reconstitution times but also durations of each reconstitution steps, which would be useful for optimizing industrial applications of food powders.

458

459 Acknowledgements

460 This research was partially supported by a grant from the International Fine Particle Research
461 Institute (IFPRI). The authors acknowledge support of the LIBio by the “Impact Biomolecules”
462 project of the “Lorraine Université d'Excellence” (Investissements d'avenir – ANR 15-004).

463

464 References

465 Bonacucina, G., Cespi, M., Palmieri, G.F., 2009. Evaluation of dissolution kinetics of hydrophilic
466 polymers by use of acoustic spectroscopy. International Journal of Pharmaceutics 377, 153–
467 158. https://doi.org/10.1016/j.ijpharm.2009.04.043

468 Conti, S., Gaisford, S., Buckton, G., Conte, U., 2006. Solution calorimetry to monitor swelling and
469 dissolution of polymers and polymer blends. Thermochimica Acta, Second Symposium on
470 Calorimetry and Chemical Thermodynamics in Campinas, Brazil 450, 56–60.
471 https://doi.org/10.1016/j.tca.2006.07.017

472 Cuq, B., Rondet, E., Abecassis, J., 2011. Food powders engineering, between knowhow and science:
473 Constraints, stakes and opportunities. Powder Technology, Special Issue: Papers presented to
474 the Symposium STPMF 2009,Science and Technology of Powders and Sintered Materials 208,
475 244–251. https://doi.org/10.1016/j.powtec.2010.08.012

476 Dokoumetzidis, A., Macheras, P., 2006. A century of dissolution research: From Noyes and Whitney to
477 the Biopharmaceutics Classification System. International Journal of Pharmaceutics 321, 1–11.
478 https://doi.org/10.1016/j.ijpharm.2006.07.011

479 Eastman, J.E., Moore, C.O., 1984. Cold-water-soluble granular starch for gelled food compositions.
480 US4465702A.

Enferad, S., Petit, J., Gaiani, C., Falk, V., Burgain, J., Kiesgen De Richter, S., Jenny, M., 2021. Effect of particle size and formulation on powder rheology. Particulate Science and Technology 39, 362–370. https://doi.org/10.1080/02726351.2020.1738605

Fang, Y., Selomulya, C., Ainsworth, S., Palmer, M., Chen, X.D., 2011. On quantifying the dissolution behaviour of milk protein concentrate. Food Hydrocolloids 25, 503–510. https://doi.org/10.1016/j.foodhyd.2010.07.030

Forny, L., Marabi, A., Palzer, S., 2011. Wetting, disintegration and dissolution of agglomerated water soluble powders. Powder Technology, 9th International Symposium on Agglomeration and 4th International Granulation Workshop, 2009 206, 72–78. https://doi.org/10.1016/j.powtec.2010.07.022

Fournaise, T., Burgain, J., Perroud, C., Scher, J., Gaiani, C., Petit, J., 2020. Impact of formulation on reconstitution and flowability of spray-dried milk powders. Powder Technology 372, 107–116. https://doi.org/10.1016/j.powtec.2020.05.085

Fournaise, T., Petit, J., Gaiani, C., 2021. Main powder physicochemical characteristics influencing their reconstitution behavior. Powder Technology 383, 65–73. https://doi.org/10.1016/j.powtec.2021.01.056

Freudig, B., Hogekamp, S., Schubert, H., 1999. Dispersion of powders in liquids in a stirred vessel. Chemical Engineering and Processing: Process Intensification 38, 525–532. https://doi.org/10.1016/S0255-2701(99)00049-5

Gaiani, Schuck, P., Scher, J., Desobry, S., Banon, S., 2007. Dairy Powder Rehydration: Influence of Protein State, Incorporation Mode, and Agglomeration. Journal of Dairy Science 90, 570–581. https://doi.org/10.3168/jds.S0022-0302(07)71540-0

Galet, L., Vu, T.O., Oulahna, D., Fages, J., 2004. The Wetting Behaviour and Dispersion Rate of Cocoa Powder in Water. Food and Bioproducts Processing 82, 298–303. https://doi.org/10.1205/fbio.82.4.298.56399

Gnagne, E., Petit, J., Gaiani, C., Scher, J., Amani, G., 2017. Characterisation of flow properties of foutou and foufou flours, staple foods in West Africa, using the FT4 powder rheometer.

508 Goalard, C., Samimi, A., Galet, L., Dodds, J.A., Ghadiri, M., 2006. Characterization of the Dispersion
509 Behavior of Powders in Liquids. Particle & Particle Systems Characterization 23, 154–158.
510 https://doi.org/10.1002/ppsc.200601024
511 Higuchi, T., 1961. Rate of Release of Medicaments from Ointment Bases Containing Drugs in
512 Suspension. Journal of Pharmaceutical Sciences 50, 874–875.
513 https://doi.org/10.1002/jps.2600501018
514 Hopfenberg, H.B., 1976. Controlled Release from Erodible Slabs, Cylinders, and Spheres, in: Controlled
515 Release Polymeric Formulations, ACS Symposium Series. AMERICAN CHEMICAL
516 SOCIETY, pp. 26–32. https://doi.org/10.1021/bk-1976-0033.ch003
517 IDF, 1987. Détermination de la dispersibilité et de la mouillabilité. International Dairy Federation,
518 Brussels, Belgium.
519 Jiang, H., Zhang, M., Adhikari, B., 2013. 21 - Fruit and vegetable powders, in: Bhandari, B., Bansal,
520 N., Zhang, Min, Schuck, P. (Eds.), Handbook of Food Powders, Woodhead Publishing Series
521 in Food Science, Technology and Nutrition. Woodhead Publishing, pp. 532–552.
522 https://doi.org/10.1533/9780857098672.3.532
523 Kim, E.H., Chen, X.D., Pearce, D., 2002. Surface characterization of four industrial spray-dried dairy
524 powders in relation to chemical composition, structure and wetting property. COLLOIDS AND
525 SURFACES B BIOINTERFACES 197.
526 Kravtchenko, T.P., Renoir, J., Parker, A., Brigand, G., 1999. A novel method for determining the
527 dissolution kinetics of hydrocolloid powders. Food Hydrocolloids 13, 219–225.
528 https://doi.org/10.1016/S0268-005X(99)00002-8
529 Lamberti, M., Geiselmann, A., Conde-Petit, B., Escher, F., 2004. Starch transformation and structure
530 development in production and reconstitution of potato flakes. LWT - Food Science and
531 Technology 37, 417–427. https://doi.org/10.1016/j.lwt.2003.10.015
532 Li, H., Grover, M.A., Kawajiri, Y., Rousseau, R.W., 2013. Development of an empirical method relating
533 crystal size distributions and FBRM measurements. Chemical Engineering Science 89, 142–
534 151. https://doi.org/10.1016/j.ces.2012.10.031

Marabi, A., Mayor, G., Burbidge, A., Wallach, R., Saguy, I.S., 2008. Assessing dissolution kinetics of powders by a single particle approach. Chemical Engineering Journal 139, 118–127. https://doi.org/10.1016/j.cej.2007.07.081

Mimouni, A., Deeth, H.C., Whittaker, A.K., Gidley, M.J., Bhandari, B.R., 2010. Investigation of the microstructure of milk protein concentrate powders during rehydration: Alterations during storage. Journal of Dairy Science 93, 463–472. https://doi.org/10.3168/jds.2009-2369

Mitchell, W.R., Forny, L., Althaus, T.O., Niederreiter, G., Palzer, S., Hounslow, M.J., Salman, A.D., 2015. Mapping the rate-limiting regimes of food powder reconstitution in a standard mixing vessel. Powder Technology, 6th International Workshop on Granulation: Granulation across the length scales 270, 520–527. https://doi.org/10.1016/j.powtec.2014.08.014

Murrieta-Pazos, I., Gaiani, C., Galet, L., Scher, J., 2012. Composition gradient from surface to core in dairy powders: Agglomeration effect. Food Hydrocolloids 26, 149–158. https://doi.org/10.1016/j.foodhyd.2011.05.003

Nernst, W., 1904. Theorie der Reaktionsgeschwindigkeit in heterogenen Systemen. Zeitschrift für Physikalische Chemie 47U, 52–55. https://doi.org/10.1515/zpch-1904-4704

Noyes, A.A., Whitney, W.R., 1897. THE RATE OF SOLUTION OF SOLID SUBSTANCES IN THEIR OWN SOLUTIONS. [WWW Document]. https://doi.org/10.1021/ja02086a003

O'Mahony, J.A., McSweeney, P.L.H., 2016. Advanced dairy chemistry. Volume 1B: Proteins: Applied aspects. Fourth Edition. Springer.

Parker, A., Vigouroux, F., Reed, W.F., 2000. Dissolution kinetics of polymer powders. AIChE Journal 46, 1290–1299. https://doi.org/10.1002/aic.690460703

Richard, B., 2012. Influence de la physico-chimie des poudres laitières et des conditions opératoires de dispersion sur la dynamique de réhydratation (thesis). http://www.theses.fr. Lille 1.

Salameh, C., Scher, J., Petit, J., Gaiani, C., Hosri, C., Banon, S., 2016. Physico-chemical and rheological properties of Lebanese kishk powder, a dried fermented milk-cereal mixture. Powder Technology 292, 307–313. https://doi.org/10.1016/j.powtec.2016.01.040

Schuck, P., Jeantet, R., Dolivet, A., 2012. Analytical Methods for Food and Dairy Powders. John Wiley & Sons.

563 Sweijen, T., Chareyre, B., Hassanizadeh, S.M., Karadimitriou, N.K., 2017. Grain-scale modelling of
564 swelling granular materials; application to super absorbent polymers. Powder Technology 318,
565 411–422. https://doi.org/10.1016/j.powtec.2017.06.015
566 Yousefi, S., Emam-Djomeh, Z., Mousavi, S.M., 2011. Effect of carrier type and spray drying on the
567 physicochemical properties of powdered and reconstituted pomegranate juice (Punica Granatum
568 L.). J Food Sci Technol 48, 677–684. https://doi.org/10.1007/s13197-010-0195-x

Reconstitution kinetics followed by granulometry

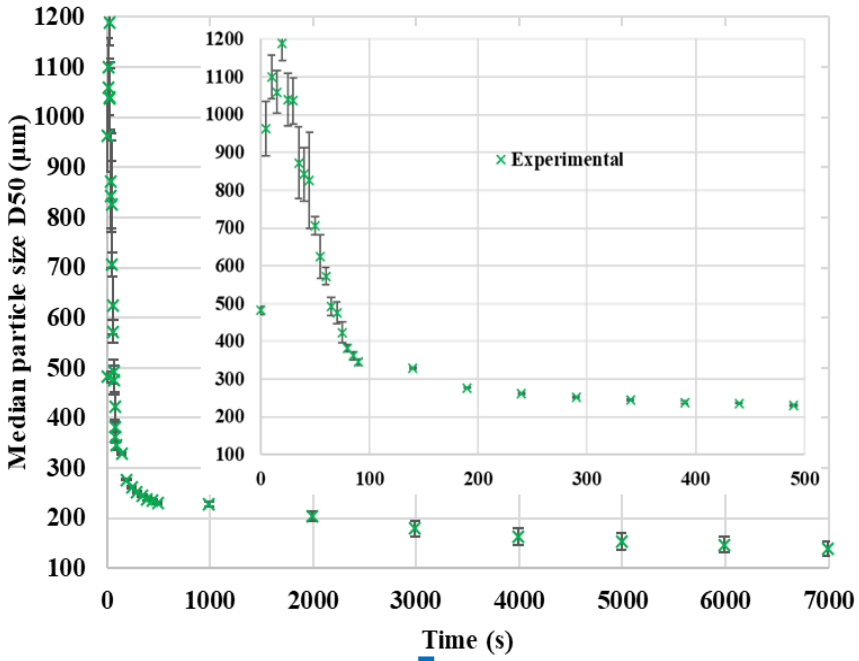

Fitting method to describe reconstitution kinetics

Dry particle size — Swelling — Dispersion — Solubilization

$$D50(t) = D50_0 + A_0\left(1 - e^{\frac{-t}{t_0}}\right) - A_1\left(1 - e^{\frac{-t}{t_1}}\right) - A_2\left(1 - e^{\frac{-t}{t_2}}\right)$$